Wang et al. 2019. *Int. J. Vehicle Structures & Systems*, 11(4), 355-361
ISSN: 0975-3060 (Print), 0975-3540 (Online)
doi: 10.4273/ijvss.11.4.02

International Journal of Vehicle Structures & Systems
Available online at www.maftree.org/eja

Intelligent Control Method for Flanking Flight of Unmanned Aerial Vehicles

Rui Wang[a], Xin-Li Yu and Nian-Chu Wu
School of Mech. Engg., Liaoning Shihua University, Fushun, China
[a]Corresponding Author, Email: 452464669@qq.com

ABSTRACT:
The angle control during the flight of UAV is the most important factor which affects its stability and safety. Since the traditional PID control method is difficult to automatically adjust the control parameters, a particle swarm optimization algorithm based on traditional PID control (PSO-PID), is proposed to construct a mathematical model of the flanking flight of the UAV. Based on the full analysis of the PID control principle, the UAV's flanking flight controller based on PID control is constructed. The particle swarm optimization algorithm is introduced to optimize the PID parameters. The simulation model is built in MATLAB to investigate the position and altitude angle change of the UAV's flank and compare it with the traditional PID control method. The experimental results show that the PSO-PID control strategy has a good control effect, which enables UAV's flanking flight to reach the specified position more quickly and accurately than traditional PID controller alone.

KEYWORDS:
Unmanned air vehicle; Intelligent control; Flanking flight; PID control; Particle swarm optimisation

CITATION:
R. Wang, X.L. Yu and N.C. Wu. 2019. Intelligent Control Method for Flanking Flight of Unmanned Aerial Vehicles, *Int. J. Vehicle Structures & Systems*, 11(4), 355-361. doi:10.4273/ijvss.11.4.02.

1. Introduction

Unmanned Aerial Vehicle (UAV) is a powered, radio-controlled or autonomous flying vehicle that performs multiple missions and can be used several times [1]. UAV has played an important role in reconnaissance, surveillance, target acquisition, target indication, communication relay, battlefield casualty assessment, communication and electronic intelligence, interference, biochemical detection, etc. [2]. To achieve radio remote control or autonomous flight of UAV, the airborne flight control technology is one of the most critical technologies. Traditionally, the basic purpose of flight control is to improve the stability and manoeuvrability of the aircraft, reduce the workload of pilots in flying the aircraft, thereby improving the ability, efficiency and effectiveness of the mission [3]. Flight control system is the core of UAV. In order to complete the autonomous flight of UAV, the control system should have good control characteristics for both the internal loop (altitude loop) and the external loop (horizontal position and height loop). The development of manned flight to UAV's autonomous flight is actually the development from flight automation to flight autonomy.

Researchers have proposed many intelligent control algorithms for the angle control of UAV's flanking flight, such as back stepping method, sliding mode control algorithm, under actuated robust control based on ESO, etc. Because of the limitation of microprocessor's computing ability when intelligent control algorithm runs complex floating-point and matrix arithmetic, it is difficult to meet the requirement of real-time flight control. Since PID control is simple, easy to implement and matured, the mainstream control strategy is mainly around the traditional PID control [4]. The exact model of the actual object is difficult to obtain and the change of weight and reconfiguration position of the UAV, even the battery voltage will affect the chess type of the controlled object. This is also the biggest obstacle in the practical application of model-based control methods such as Linear Quadratic (LQ), feedback linearization and back stepping. The input of the mainstream model used in the research of the unmanned system is not consistent with the control input signal of the actual system. The actual control input of the object is the throttle signal of the electronic governor and there is still a dynamic process between the throttle, thrust and torque signals. Some signals, such as total thrust, which are dependent on the design of nonlinear controllers, cannot be directly measured in practical systems.

Although the PID controller occupies a high proportion in practical application, it is a single-input and single-output controller designed for hovering balance point. Although it can meet the requirements of general flight mission, it cannot guarantee the stability of the system in a wide range. In fast track mode such as large altitude and high angular rate, the nonlinear characteristics of the controlled object will lead to the degradation of control quality. In addition, PID controllers generally contain multiple control loops. For new models, there are some problems such as tedious parameter tuning and strong experience dependence. In the field of motion control, the control quality required is high and the control object is more complex. Especially in the industrial process with strong disturbance, the parameters of the controller are difficult because of the limitations of the PID controller, so that automatic

adjustment cannot achieve the desired control effect [5-6]. Therefore, aiming at the limitation of conventional PID controller, this paper proposes a control optimization algorithm based on particle swarm optimization (PSO) and traditional PID control. The performance of the controller is verified by simulation. The experimental results show that the algorithm has a good control effect.

2. Means and methods

UAV's flank is a non-linear, multi-variable, strong coupling controlled object. The design of its flight system is mainly aimed at its strong coupling, instability and sensitivity to external disturbances and other dynamic characteristics to propose appropriate algorithms to achieve the goal of stable flight control. At the same time, because the control of flight altitude is the loop of displacement trajectory control, a good altitude controller design scheme can not only ensure the stable flight of UAV's flanks in the air, but can also control the flight displacement trajectory of the flanks.

2.1. Mathematical model

According to Newton's second law, the equation of line motion in the inertial coordinate system is given by,

$$\vec{F}^O = d(m\vec{V}^O)/dt \tag{1}$$

Where $\vec{F}^O$ represents the resultant external forces acting on the flanks, including the lift generated by the flanks, air drag f^O and the weight of the flanks themselves. The mathematical expression is given by,

$$\vec{F}^O = R\vec{T}^O + \vec{f}^O - mg\vec{z} \tag{2}$$

Where m represents the mass of the flanks and $\vec{V}^O = [u \quad v \quad w]^T$ is the velocity vector of the UAV relative to the inertial coordinate system. The total lift of the flanks can be expressed as,

$$\vec{T}^O = \begin{bmatrix} 0 & 0 & \sum_{i=1}^{4} T_i \end{bmatrix}^T \tag{3}$$

Where $T_i = \partial\Omega_i{}^2, \quad i = 1,2,3,4,$ represents the lift generated by each rotor and is proportional to the square of the rotor speed. ∂ represents the lift coefficient of the rotor. Ω_i represents the speed of the i[th] rotor [7]. The mathematical relationship is given by,

$$\vec{f}^O = -C_f \rho_f S \left|\vec{V}\right| \vec{V}/2 = -\sigma \left|\vec{V}\right| \vec{V} \tag{4}$$

Where C_f is the air drag coefficient. ρ_f is the atmospheric density and S is the cross-sectional area of flanks facing the wind. The equation of linear motion of the flanks can be obtained using,

$$m\begin{bmatrix} \dot{u} \\ \dot{v} \\ \dot{w} \end{bmatrix} = R\begin{bmatrix} 0 \\ 0 \\ \sum_{i=1}^{4} T_i \end{bmatrix} - \sigma \left|\vec{V}\right| \vec{V} - mg\begin{bmatrix} 0 \\ 0 \\ 1 \end{bmatrix} \tag{5}$$

At the same time, through the coordinate transformation, the linear displacement of the flanks from the airframe coordinate system to the three coordinate axes in the inertial coordinate system can be obtained using,

$$\begin{cases} \ddot{x} = (C_\psi S_\theta C_\varphi + S_\psi S_\varphi)\sum_{i=1}^{4} \partial\Omega_i^2/m - \sigma\dot{x}^2/m \\ \ddot{y} = (S_\psi S_\theta C_\varphi - S_\varphi C_\psi)\sum_{i=1}^{4} \partial\Omega_i^2/m - \sigma\dot{y}^2/m \\ \ddot{z} = C_\theta C_\varphi \sum_{i=1}^{4} \partial\Omega_i^2/m - \sigma\dot{z}^2/m - g \end{cases} \tag{6}$$

$$\begin{bmatrix} \dot{x} \\ \dot{y} \\ \dot{z} \end{bmatrix} = R\begin{bmatrix} u \\ v \\ w \end{bmatrix} = \begin{bmatrix} C_\psi C_\theta & C_\psi S_\theta S_\varphi - C_\varphi S_\psi & C_\psi S_\theta C_\varphi + S_\psi S_\varphi \\ S_\psi C_\theta & SS_\theta S_\varphi + C_\varphi C_\psi & S_\psi S_\theta C_\varphi - S_\varphi C_\psi \\ -S_\theta & C_\theta S_\varphi & C_\theta C_\varphi \end{bmatrix}\begin{bmatrix} u \\ v \\ w \end{bmatrix} \tag{7}$$

$$\begin{cases} \dot{x} = uC_\psi C_\theta + v(C_\psi S_\theta S_\varphi - C_\varphi S_\psi) + w(C_\psi S_\theta C_\varphi + S_\psi S_\varphi) \\ \dot{y} = uS_\psi C + v(S_\psi S_\theta S_\varphi + C_\varphi C_\psi) + w(S_\psi S_\theta C_\varphi - S_\varphi C_\psi) \\ \dot{z} = -uS_\theta + vC_\theta S_\varphi + wC_\theta C_\varphi \end{cases} \tag{8}$$

The external forces acting on the flanks mainly include the rotating moments, gyroscopic effects and drag moments. However, because of the structural symmetry of the flanks, the sum of the drag moments can be regarded as zero. In rolling, pitching and yawing motions, there are some differences among the three rotational forms. Through force analysis, the moment of lift difference along x, y and z axis are expressed as follows:

$$\begin{cases} \Gamma_\varphi = l\partial(\Omega_4^2 - \Omega_2^2) \\ \Gamma_\theta = l\partial(\Omega_1^2 - \Omega_3^2) \\ \Gamma_\psi = \tau(\Omega_2^2 + \Omega_4^2 - \Omega_1^2 - \Omega_3^2) \end{cases} \tag{9}$$

Where l is the distance between the centre of mass of the body and the rotation axis of the rotating flanks. ∂ is the lift coefficient and τ is the reverse torque coefficient.

Considering the gyroscopic effect of the flanks and the good symmetry of the flanks [8], the moment of inertia of the rigid body of the flanks to the fixed axis can be found using,

$$I = \begin{bmatrix} I_{xx} & 0 & 0 \\ 0 & I_{yy} & 0 \\ 0 & 0 & I_{zz} \end{bmatrix} \tag{10}$$

$W = [\alpha \; \beta \; \gamma]^T$ is defined as the angular velocity vector that rotates around the axis of the body coordinate system. In practical engineering applications, U_1, U_2, U_3, U_4 is generally defined as the input control of the vertical motion, roll motion, pitch motion and yaw motion in UAV's flanking flight and computed as follows,

$$\begin{bmatrix} U_1 \\ U_2 \\ U_3 \\ U_4 \end{bmatrix} = \begin{bmatrix} \partial(\Omega_1^2 + \Omega_2^2 + \Omega_3^2 + \Omega_4^2) \\ \partial(\Omega_4^2 - \Omega_2^2) \\ \partial(\Omega_1^2 - \Omega_3^2) \\ \tau(\Omega_2^2 + \Omega_4^2 - \Omega_1^2 - \Omega_3^2) \end{bmatrix} \tag{11}$$

At the same time, considering the complexity of the controller design, we can ignore some factors which have little influence to reduce the difficulty of the controller design. Firstly, we assume that the UAV is flying at a slow speed in a breezy or windless ideal weather condition, so the effect of air drag can be ignored [9]. Secondly, considering the smaller rotor size of the UAV, the gyroscopic effect produced by the UAV can be neglected in a simple flight test. Furthermore, the angular velocity $[\alpha\ \beta\ \gamma]^T$ of the UAV rotating around each axis of the airframe coordinate system is approximately equal to the change rate of the altitude angle $\left[\dot{\phi}\ \dot{\theta}\ \dot{\psi}\right]^T$ in the inertial coordinate system. Finally, the general mathematical model of the flanks is obtained as follows,

$$\begin{cases} \ddot{x} = (C_\psi S_\theta C_\varphi + S_\psi S_\varphi)U_1 / m \\ y = (S_\psi S_\theta C_\varphi + S_\varphi S_\psi)U_1 / m \\ \ddot{z} = C_\theta C_\varphi U_1 / m - g \\ \ddot{\varphi} = \dfrac{I_{yy} - I_{zz}}{I_{xx}}\dot{\theta}\dot{\psi} + \dfrac{l}{I_{xx}}U_2 \\ \ddot{\theta} = \dfrac{I_{zz} - I_{xx}}{I_{yy}}\dot{\varphi}\dot{\psi} + \dfrac{l}{I_{yy}}U_3 \\ \ddot{\psi} = \dfrac{I_{xx} - I_{yy}}{I_{zz}}\dot{\theta}\dot{\varphi} + \dfrac{l}{I_{zz}}U_4 \end{cases} \tag{12}$$

2.2. PID controller

PID is a typical linear controller. The PID controller consists of proportional unit, integral unit and differential unit. The typical single-stage PID controller is shown in Fig 1. The control laws of PID are as follows:

$$u(t) = K_P\left[e(t) + \frac{1}{T_I}\int_0^t e(t)dt + T_D\frac{de(t)}{dt}\right] \tag{13}$$

Where K_P is the ratio coefficient. T_I is the integral time constant. T_D is the differential time constant. $e^{(t)}$ is the deviation between the given value $r(t)$ and the actual output value $y(t)$. In the actual control system, we need to adjust the control parameters according to the specific requirements, until the system meets the performance requirements [10].

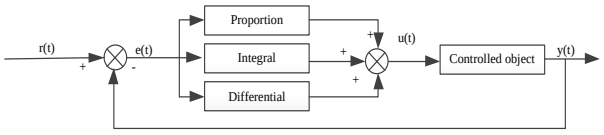

Fig. 1: Block diagram of single-stage PID controller

From the dynamic model of UAV's flanks, it is a 4-input-6-output control system with multi-variable, under actuated, nonlinear and strong coupling. When the altitude sensor of UAV's flanks is disturbed by wind or magnetic field, the data collected sometimes will be distorted [11]. In this case, the Euler altitude angle of UAV flanks cannot be calculated accurately. Therefore, the double-loop cascade control strategy is adopted. This takes the position control as the outer loop of the system and the altitude control as the inner loop of the system. The double-loop cascade control strategy not only removes the obstacles caused by the under actuation of the system to the controller design, but also removes the coupling between the inner loop altitude control and the outer loop position control. The structure of PID control system based on double-loop cascade control strategy for UAV's flanks is shown in Fig. 2.

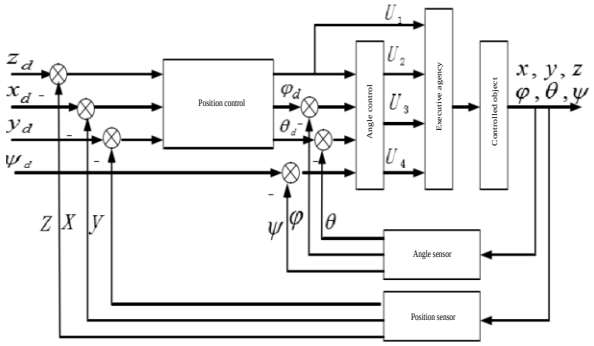

Fig. 2: Double-loop cascade PID control structure for UAV's flank

Position controller is mainly to make the UAV to position accurately and quickly in accordance with the established requirements of smooth flight. The position controller consists of two control channels, the horizontal controller and the altitude controller. The purpose of the horizontal controller is to calculate the initial altitude angle of the UAV accurately and then adjust the altitude by the altitude controller. The purpose of the altitude controller is to hover the UAV's flanks to the specified height [12]. Firstly, the expected position value of the system is defined as (x_d, y_d, z_d), and the actual position value is (x, y, z). The deviation between them is used as the input signal of PID control. According to the dynamics model Eqn. (12) and PID control law Eqn. (13), the control algorithm can be obtained as follows:

$$\begin{cases} \ddot{x} = K_{px}(x_d - x) + K_{ix}\int(x_d - x)dt + K_{dx}\dfrac{d(x_d - x)}{dt} \\ \ddot{y} = K_{py}(y_d - y) + K_{iy}\int(y_d - y)dt + K_{dy}\dfrac{d(y_d - y)}{dt} \\ \ddot{z} = K_{pz}(z_d - z) + K_{iz}\int(z_d - z)dt + K_{dz}\dfrac{d(z_d - z)}{dt} \end{cases} \tag{14}$$

Where $\ddot{Z}$ is the acceleration of the specified height which is used as the input signal of the lift U_1. From Eqn. (12) of the mathematical model of the UAV's flank, we can see the relationship between the acceleration of the height and U_1. Combining Eqn. (3) and Eqn. (14), the lift U_1 is derived as,

$$U_1 = m\left[K_{pz}(z_d - z) + K_{iz}\int(z_d - z)dt + K_{dz}(z_d - z) + g\right] / C\varphi C\theta \tag{15}$$

The expression of $\ddot{x}$ in Eqn. (12) is multiplied by $\sin\varphi$ on both sides and the expression of $\ddot{y}$ is multiplied by $\cos\varphi$ on both sides. Then the two expressions are subtracted to obtain the following,

$$m\ddot{x}\sin\psi - m\ddot{y}\cos\psi = U_1\sin\varphi \tag{16}$$

$$\varphi_d = \arcsin\left(\frac{m}{U_1}(\ddot{x}\sin\psi - \ddot{y}\cos\psi)\right) \tag{17}$$

The terms $\ddot{x}$ and $\ddot{y}$ are obtained through a series of transformations as,

$$\theta_d = \arcsin\left(\frac{m}{U_1\cos\phi}(\ddot{x}\cos\psi + \ddot{y}\cos\psi)\right) \tag{18}$$

The desired altitude angle of the system is defined as $(\varphi_d, \theta_d, \psi_d)$. The actual altitude angle is (φ, θ, ψ). The deviation between them is used as the input signal of the PID controller [13]. The control algorithm is as follows:

$$\begin{cases} \ddot{\varphi}=K_{p\varphi}(\varphi_d-\varphi)+K_{i\varphi}\int(\varphi_d-\varphi)dt+K_{d\varphi}\dfrac{d(\varphi_d-\varphi)}{dt} \\ \ddot{\theta}=K_{p\theta}(\theta_d-\theta)+K_{i\theta}\int(\theta_d-\theta)dt+K_{d\theta}\dfrac{d(\theta_d-\theta)}{dt} \\ \ddot{\psi}=K_{p\psi}(\psi_d-\psi)+K_{i\psi}\int(\psi_d-\psi)dt+K_{d\psi}\dfrac{d(\psi_d-\psi)}{dt} \end{cases} \tag{19}$$

When UAV is in low speed and hovering state, the change of angular rate is very small and the cross term is very close to zero [14]. Therefore we can further simplify the last three items in Eqn. (12) as follows,

$$\begin{cases} \ddot{\varphi}=lU_2/I_{xx} \\ \ddot{\theta}=lU_3/I_{yy} \\ \ddot{\psi}=lU_4/I_{zz} \end{cases} \tag{20}$$

The expressions of four control inputs U_1, U_2, U_3, U_4 for UAV's flanks can be obtained by combining Eqns (15), (17) and (18) as,

$$\begin{cases} U_1 = m\left[K_{pz}(z_d-z)+K_{iz}\int(z_d-z)dt+K_{dz}(\dot{z}_d-\dot{z})+g\right]/C\varphi C\theta \\ U_2 = I_{xx}\left[K_{p\varphi}(\varphi_d-\varphi)+K_{i\varphi}\int(\varphi_d-\varphi)dt+K_{d\varphi}\dfrac{d(\varphi_d-\varphi)}{dt}\right]/l \\ U_3 = I_{yy}\left[K_{p\theta}(\theta_d-\theta)+K_{i\theta}\int(\theta_d-\theta)dt+K_{d\theta}\dfrac{d(\theta_d-\theta)}{dt}\right]/l \\ U_4 = I_{zz}\left[K_{p\psi}(\psi_d-\psi)+K_{i\psi}\int(\psi_d-\psi)dt+K_{d\psi}\dfrac{d(\psi_d-\psi)}{dt}\right] \end{cases} \tag{21}$$

The position controller loop U_1 and altitude controller U_2, U_3, U_4 are input into the motor system and then the altitude angle measurement signal and the position change signal are used as the feedback signals of the system respectively in the object model of the UAV's flank, thus forming the closed-loop system. The stability of the system is achieved by adjusting the parameters of PID. According to the linear mathematical model of UAV's flank, Eqn.(20) and the first three terms of Eqn. (12), the measured system parameters and the double-loop cascade PID control strategy designed above, the components of the simulation system as established in MATLAB are shown in Figs. 3 to 6.

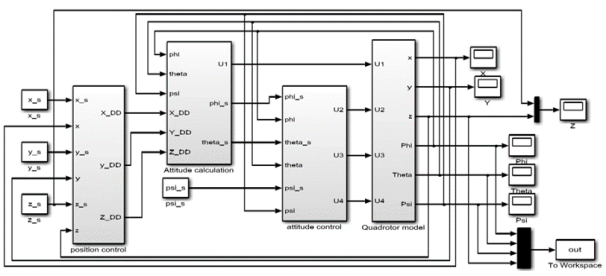

Fig. 3: Simulation diagram of control system

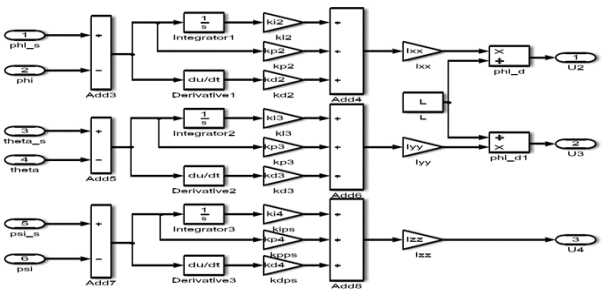

Fig. 4: Internal diagram of angle control system

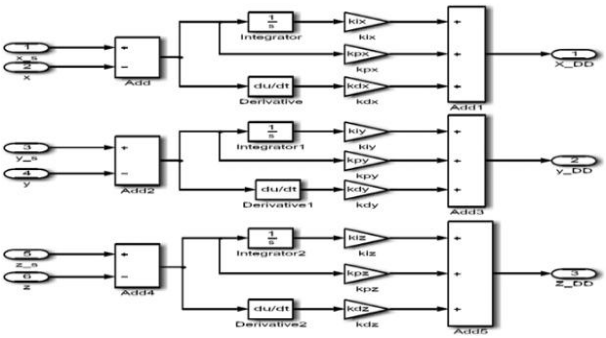

Fig. 5: Internal diagram of position control system

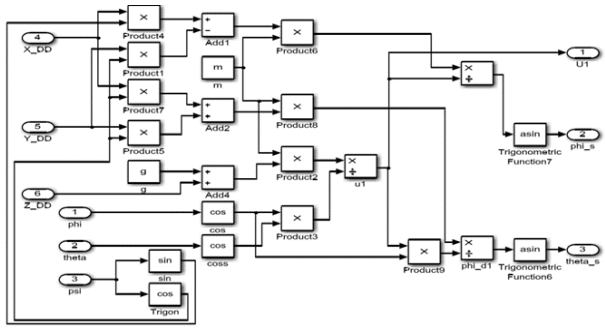

Fig. 6: Internal diagram of angle calculation control system

2.3. PSO-PID controller

The control performance of the PID controller depends on whether the parameters of p_k, i_k and d_k are reasonable or not. Therefore, it is very important to optimize the parameters of the system. However, the parameters of the PID controller are mainly adjusted manually at present, which is not only time-consuming, but also cannot ensure the optimal control quality of the system. In this section, PSO is used to optimize the parameters of PID controller. The optimization algorithm flow based on PSO is shown in Fig. 7. Optimizing the PID control strategy of UAV's flanking flight is to select the suitable control parameter k_p, k_i, k_d so as to achieve the optimal error performance index. The ITAE error performance index is given as,

$$J = \int_0^\infty t\left|e(t)\right|dt \tag{22}$$

Fig. 8 shows the schematic of the optimization design process of PSO algorithm.

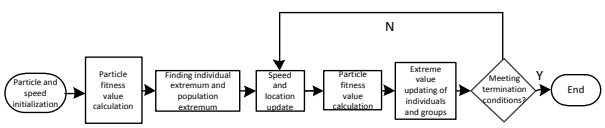

Fig. 7: Optimization algorithm flow based on PSO algorithm

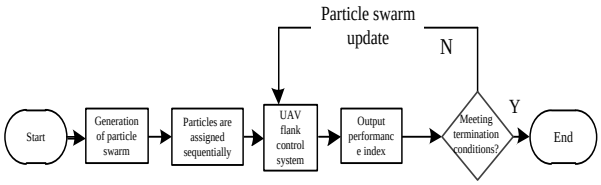

Fig. 8: Schematic diagram of PSO algorithm for optimizing PID

The speed and location of particles are taken as:

$$v_{t+1} = \omega v_t + c_1 r_1 (P_t - x_t) + c_2 r_2 (G_t - x_t) \quad (23)$$

$$x_{t+1} = x_t + v_{t+1} \quad (24)$$

Where v is the velocity of the particle. c_1 and c_2 are the acceleration constants. x is the position of the particle. ω is the inertia factor. r_1 and r_2 are the random number of [0, 1] interval. P_t is the optimal position of the particle as of the current search. G_t is the optimal position of the entire particle swarm as of the current search. The control principle is shown in Fig. 9. The PSO-PID control simulation system as set up in MATLAB is shown in Figs. 10 to 12. PSO algorithm optimization process is as follows:

1. Randomly generate all particles position and speed to determine P_t and G_t.
2. Compare the fitness of each particle with that of P_t,. the condition is satisfied, the fitness is taken as the current P_t.
3. Compare the fitness of each particle with that of G_t, if the condition is satisfied, the fitness of each particle is regarded as the current G_t.
4. Update the velocity and position of particles according to Eqns. (23) and (24).
5. If the obtained parameters have not met the conditions, return to step (2) again, otherwise terminate to get the optimal solution.

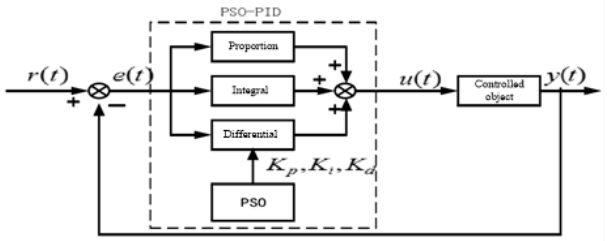

Fig. 9: Introduction of the control chart of PSO algorithm

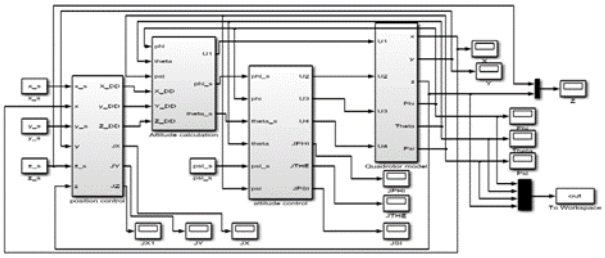

Fig. 10: Simulation diagram of PSO-PID control

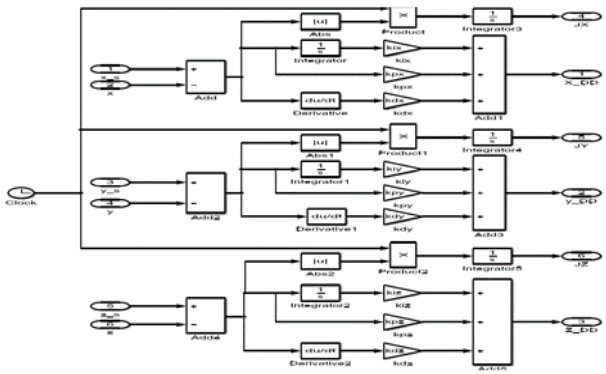

Fig. 11: Simulation diagram of PSO-PID position control

After designing the PID controller for UAV's flanking flight, the PSO algorithm is introduced to optimize the PID control parameter K_p, K_i, K_d.

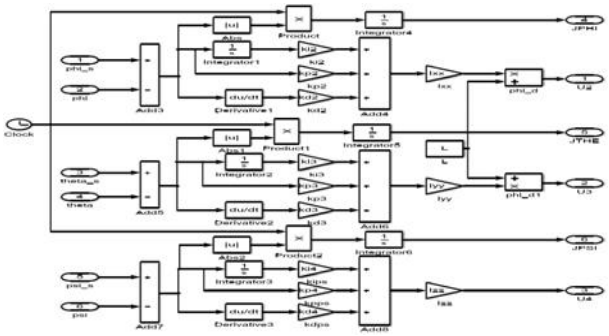

Fig. 12: Simulation diagram of PSO-PID altitude angle control

3. Results and discussion

The simulation model is established in MATLAB. The parameters for the PSO and UAV flank design are given in Table 1. According to experimental values, the range of the 3 parameters to be optimised is determined as [0, 150]. The performance index curve of optimal parameter change obtained after running the simulation program for optimization is shown in Fig. 13. As the ITAE is decreasing, PSO is searching for the optimal parameters. PSO iterative optimization has been basically stable after 25 steps, and computational efficiency is relatively high. As can be seen from Fig. 14, for the pitch angle of UAV's flanks, the PID controller optimized by PSO iteration can control the pitch angle very well and can meet the control requirements. The results of the PSO-PID controller and PID controller are compared and analysed to illustrate their advantages. At time t = 0, the UAV is in position [0, 0, 0] and the target position is [1, 1, 1]. During this period, the altitude angle of the UAV's flanking flight changes. The x, y and z directions' flanking are shown in Figs. 15 to 20.

Table 1: System parameters for designing UAV flanks

Parameter	Value	Parameter	Value
Particle swarm size	30	m(kg)	1.24
Max. No. of iterations	50	l(m)	0.38
Parameter to be optimised	3	R(m)	0.12
Inertia factor, w	0.8	I_{xx}(kgm^2)	2.482×10^{-3}
Max. Fitness value	0.1	I_{yy}(kgm^2)	2.513×10^{-3}
Velocity range	[-1, 1]	I_{zz}(kgm^2)	5.867×10^{-3}
$c_1 = c_2$	2	t(Nms^2)	3.24×10^{-6}

All the results are compared more accurately in terms of peak time, maximum dynamic deviation and adjustment time and summarised in Table 2. The position and altitude angle of UAV's flanks under PSO-PID control are better than those under conventional PID control. The peak time is generally shortened by 0.5s-

0.7s. The maximum dynamic deviation of position change is reduced by 0.05-0.11. The maximum dynamic deviation of altitude angle change is reduced by 0.2-0.3. The adjustment time of position and altitude changes is shortened by 1.7s-3.9s. Therefore, compared with the traditional PID control, PSO-PID control strategy can not only adjust the parameters more quickly, but also has better flight performance under its control.

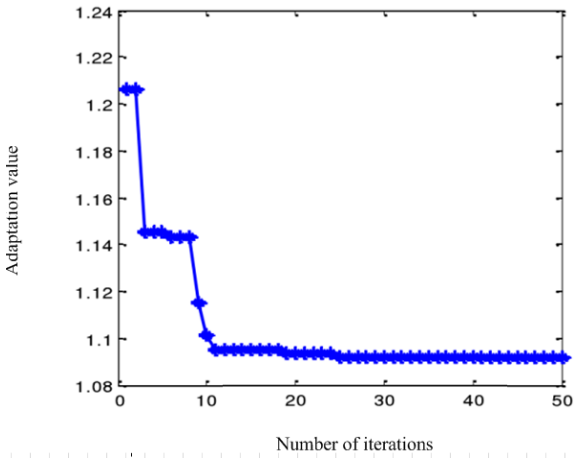

Fig. 13: Performance index ITAE

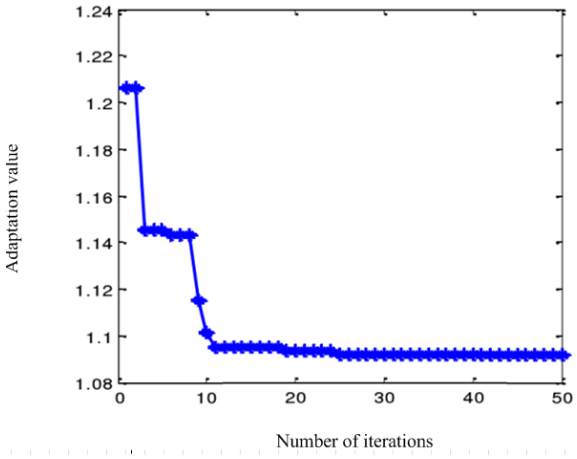

Fig. 13: Performance index ITAE

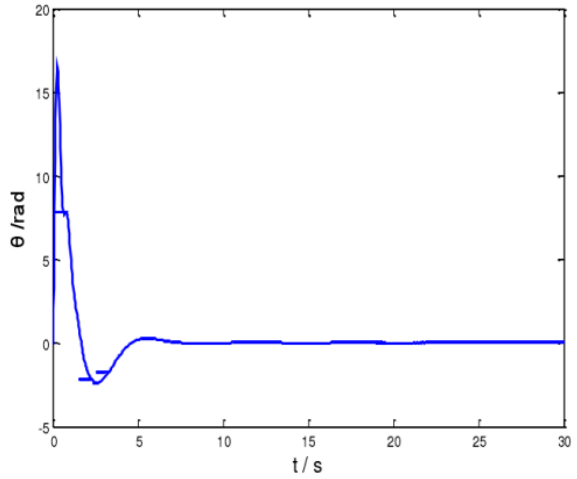

Fig. 14: Variation of pitch angle after PSO

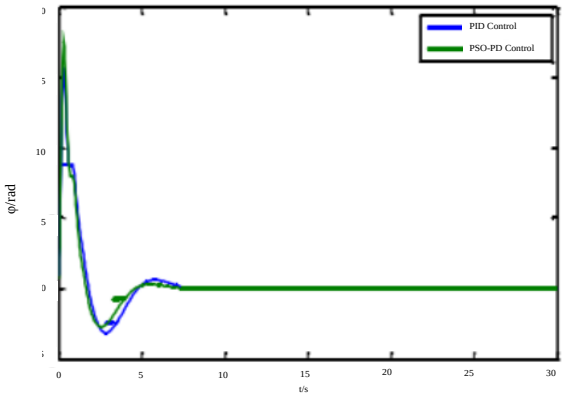

Fig. 15: Variation curve of roll angle φ

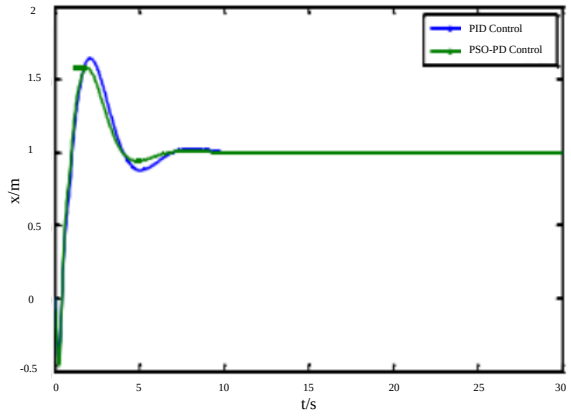

Fig. 16: Variation curve of x direction flanking

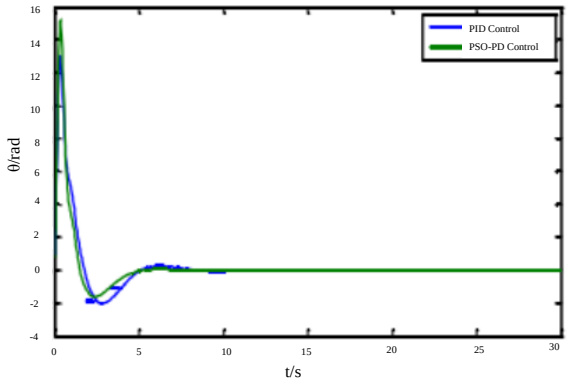

Fig. 17: Variation curve of pitch angle θ

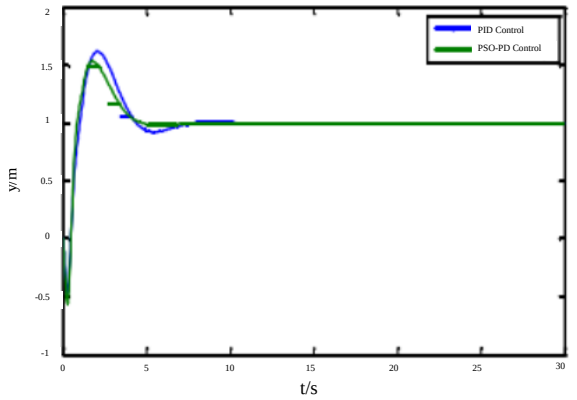

Fig. 18: Variation curve of y axis direction flanking

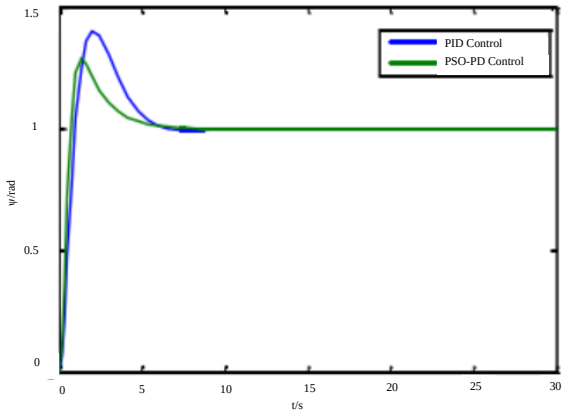

Fig. 19: Variation curve of yaw angle ψ

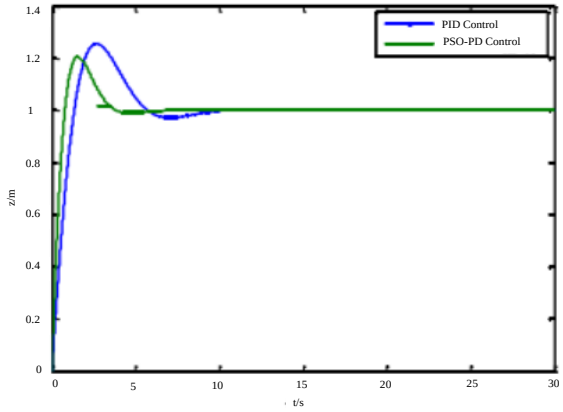

Fig. 20: Variation curve of z axis direction flanking

Table 2: Comparison of performance index by PID control and PSO-PID control

Performance index	control strategy	X-Position	Y-Position	Z-Position	φ	θ	ψ
Peak time tp (s)	PID	2.5	2.6	2.2	2.5	2.6	3.0
	PSO-PID	2.0	2.0	1.5	2.0	2.0	2.5
Max. dynamic deviation A ($\|\varepsilon\|$)	PID	0.65	0.60	0.25	4.00	1.80	0.42
	PSO-PID	0.58	0.49	0.20	3.80	2.10	0.25
Adjustment time ts (s)	PID	8.0	8.5	9.7	9.0	8.5	7.5
	PSO-PID	6.0	6.0	5.8	6.0	6.0	5.8

4. Conclusions

In order to solve the problem, traditional PID control method is difficult to automatically adjust control parameters, a control optimization algorithm based on particle swarm optimization and traditional PID control is proposed. A simulation model is established in MATLAB to investigate the position changes and altitude angles of UAV's flank. The experimental results show that the PSO-PID control strategy has good control effect and can enable the UAV's flank to reach the designated location more quickly and accurately than conventional PID control.

REFERENCES:

[1] Y. Zeng and H. Guo. 2018. An Euler angle calculation method for Tailsitter UAV, *Chinese Automation Congress*. https://doi.org/10.1109/CAC.2017.8242878.

[2] B. Yuksek, A. Vuruskan, U. Ozdemir, M.A. Yukselen and G. Inalhan. 2016. Transition flight modeling of a fixed-wing VTOL UAV. *J. Intelligent & Robotic Syst.* 84(1), 83-105. https://doi.org/10.1007/s10846-015-0325-9.

[3] S.J Lee and H.J. Kim. 2017. Autonomous swing-angle estimation for stable slung-load flight of multi-rotor UAVs, *Int. Conf. Robotics and Automation.*, 4576-4581. https://doi.org/10.1109/ICRA.2017.7989532.

[4] S. Jain and C. Kamali. 2016. Reconstruction of aerodynamic angles from flight data for "Slybird" Unmanned Aerial Vehicle (UAV), *Indian Control Conf.*, https://doi.org/10.1109/INDIANCC.2016.7441136.

[5] V.S. Chipade, Abhishek, M. Kothari and R.R. Chaudhari. 2018. Systematic design methodology for development and flight testing of a variable pitch quadrotor biplane VTOL UAV for payload delivery, *Mechatronics*, 55, 94-114. https://doi.org/10.1016/j.mechatronics.2018.08.008.

[6] D. Chao, H. Bai and J. Zeng. 2017. Nonlinear stabilization control of tilt rotor UAV during transition flight based on HOSVD, *Guidance, Navigation & Control Conf.*, 154-159. https://doi.org/10.1109/CGNCC.2016.7828775.

[7] W. Jung, S. Lim, D. Lee and H. Bang. 2016. Unmanned aircraft vector field path following with arrival angle control, *J. Intelligent and Robotic Systems*, 84(1-4), 311-325. https://doi.org/10.1007/s10846-016-0332-5.

[8] S.F. Ahmed, F.A. Warsi, K. Kadir and Z. Janin, 2016. Non-liner model predictive controller based incidence angle estimation and controlling of fixed wing UAV under noisy and delayed sensor's feedback condition, *Int. Conf. Smart Instr., Measurement and Applications*, 1-6. https://doi.org/10.1109/ICSIMA.2015.7559023.

[9] A. Wenz, T.A. Johansen and A. Cristofaro. 2016. Combining model-free and model-based angle of attack estimation for small fixed-wing UAVs using a standard sensor suite, *Int. Conf. Unmanned Aircraft Sys.*, 624-632. https://doi.org/10.1109/ICUAS.2016.7502583.

[10] J.J. Xiong, G. Zhang. 2016. Sliding mode control for a quadrotor UAV with parameter uncertainties, *Int. Conf. Control, Automation and Robotics*, 207-212. https://doi.org/10.1109/ICCAR.2016.7486727.

[11] R. Bai and M. Zhang. 2018. An art district system dynamics model of diversified operation based on game theory, *J. Discrete Mathematical Sci. and Cryptography*, 21(4), 1019-1030. https://doi.org/10.1080/09720529.2018.1479178.

[12] P. Narasimman. 2018. Solution and stability of a generalized k-additive functional equation, *J. Interdisciplinary Mathematics*, 21(1), 171-184. https://doi.org/10.1080/09720502.2015.1086113.

[13] A. Vinogradov, Y. Matveev, I. Ivanikin, R. Lubchenco, and P. Titov. 2017. The influence of material properties on the parameters of piezoelectric micropumps, *J. Mech. Engg. Research and Developments*, 40(4), 699-705, https://doi.org/10.7508/jmerd.2017.04.017.

[14] X. Yan, H. Zhang, X. Zhou, Z. Shuai, Q. Ziyang and Z. Guoqing. 2016. Environment monitoring system based on four-rotor UAV, *Automation and Instrumentation*, 2016(10), 85-86.